Article

Improve Building Façades in Open Lidar Data using Ground Imagery

Shenman Zhang [1,*], Pengjie Tao [1]

[1] School of Remote Sensing and Information Engineering, Wuhan University, 430079, Wuhan, China

* Correspondence: smzhang@whu.edu.cn

Abstract: Recent advances in open data initiatives allow us to free access to a vast amount of open LiDAR data in many cities. However, most of these open LiDAR data over cities are acquired by airborne scanning, where the points on façades are sparse or even completely missing due to the viewpoint and object occlusions in the urban environment. Integrating other sources of data, such as ground images, to complete the missing parts is an effective and practical solution. This paper presents an approach for improving open LiDAR data coverage on building façades by using point cloud generated from ground images. A coarse-to-fine strategy is proposed to fuse these two different sources of data. Firstly, the façade point cloud generated from terrestrial images is initially geolocated by matching the SFM camera positions to their GPS meta-information. Next, an improved Coherent Point Drift algorithm with normal consistency is proposed to accurately align building façades to open LiDAR data. The significance of the work resides in the use of 2D overlapping points on the outline of buildings instead of limited 3D overlap between the two point clouds and the achievement to a reliable and precise registration under possible incomplete coverage and ambiguous correspondence. Experiments show that the proposed approach can significantly improve the façades details of buildings in open LiDAR data and improving registration accuracy from up to 10 meters to less than half a meter compared to classic registration methods.

Keywords: Open LiDAR; Terrestrial Images; Building Reconstruction; Point Cloud Registration

---

1. Introduction

In recent years, there has been a significant push from the open data initiatives in many North American cities [1–3] or the large projects such as Infrastructure for Spatial Information in the European Community (INSPIRE) [4,5] proposed by European Commissions to provide vast amounts of open datasets that also include open LiDAR data [6,7]. Nowadays, open LiDAR data covering most parts of Europe and North America are already available for the public. Due to the free access to these open LiDAR data, new avenues of research for students, researchers, and other LiDAR data user community have been opened [8–10]. However, these open LiDAR data are often sparse and incomplete, or even entirely void on the façades due to the viewpoint and occlusions in the urban environment. This problem makes it difficult to achieve fine building reconstruction with high levels of detail (LoD) [11].

Recently, ground imagery capture devices such as off-the-shelf digital cameras, smartphones with GPS and digital compass have become ever prevalent. They allow us to acquire a number of high-resolution images of the building façade through crowd-sourcing at low cost. Additionally, the state-of-the-art Structure-from-Motion (SfM) and Multi-View Stereo (MVS) reconstruction techniques [12–16] allow us to process these ground images so as to recover façades information in fine detail and precision. Considering that ground images are complementary to open LiDAR data

Peer-reviewed version available at Remote sensing 2019, 11, 420; doi:10.3390/rs11040420

in terms of façade details, fusing façade point cloud generated from ground images into open LiDAR data is a promising way to improve open LiDAR data on the details of façade.

Various researches have been studied on the fusion of multiple sources of data to reconstruct buildings with rooftops and façades information. Boulaassal et al. [17] combined airborne LiDAR scanning (ALS), terrestrial LiDAR scanning (TLS) and vehicle LiDAR scanning (VLS) data to produce reliable 3D building models, however, the high costs of using several kinds of laser scanners limited the applications of this technique. Besides, the success of this combination relied on a controlled and corrected geo-referencing of GPS before processing. Shan et al. [18] addressed this problem using a viewpoint-dependent matching method so that the aerial and the ground images could be accurately matched to generate high-quality multi-view stereo models. However, this depends on the quality of ground imagery and its similar appearance with the aerial images. Wang et al. [19] proposed a system for aligning 3D SfM point clouds produced from Internet imagery to existing Google Earth 3D models and Google Street View photos. Their method relied on the quality of Google Earth 3D models which often is not very credible and may vary in different cities.

Essentially, the fusion of façade point cloud and open LiDAR data is a process of point set registration that maps one point set to the other according to their correspondence. Point set registration is a crucial step in many computer vision and photogrammetry tasks including stereo matching [20], medical imaging [21], heritage reconstruction [22], shape retrieval [23] and industrial applications [24]. Iterative Closest Point (ICP) [25] is the most widely used and classic point sets registration algorithm due to its simplicity and low computational complexity. It iteratively assigns correspondence based on the closest distance criterion and finds the least-squares transformation between the pair of point sets until a local minimum is reached. A major drawback of ICP algorithm is that it demands an accurate initial guess of the correspondence between two point sets. Otherwise, it may fall into a local minimum or even be non-convergent. A lot of ICP-based variants have been proposed to address the weaknesses [26–30]. Myronenko et al. proposed a probabilistic-based point set registration algorithm [31] which is called Coherent Point Drift (CPD). CPD considers the alignment of a pair of point sets as a probability density estimation problem where one point set represents the Gaussian Mixture Model (GMM) centroids, and the other one represents the data points. The rigid transformation that aligns GMM centroids to data points is obtained by maximizing the GMM posterior probability for data points at the optimum. The CPD algorithm, which exhibits a linear computational complexity, outperforms most state-of-the-art algorithms and achieves promising results with respect to conditions of noise, outliers, and missing points.

Nonetheless, the alignment between façade point cloud and open LiDAR data remains a problem because of (1) inevitable noise points in facade point cloud, including noise points from SfM and MVS procedure and noise points of other ground objects such as trees, lamp-posts, and passers-by; (2) limited overlaps between the two point clouds; (3) their large density difference; and (4) their large initial offset. All these issues lead to a challenge to traditional point sets registration algorithms.

This paper presents a novel method for improving open LiDAR data on the building façade using the façade point cloud generated from ground images. Firstly, to reduce the significant differences in rotation, scale, and translation between the two kinds of point cloud, we achieve initial geolocation of façade point cloud by matching the SfM camera positions to their GPS imaging meta-data. Then, a modified CPD algorithm with normal consistency is proposed to achieve precise registration by making full use of similarity on 2D outlines of buildings. The significance of the work resides in the best use of the most likely overlap between the two point clouds and the achievement to a reliable and precise registration under possible incomplete coverage and ambiguous correspondence. The overview of the proposed method is illustrated as Figure 1.

Preprints (www.preprints.org) | NOT PEER-REVIEWED | Posted: 16 October 2018 doi:10.20944/preprints201810.0354.v1

Peer-reviewed version available at *Remote sensing* **2019**, *11*, 420; doi:10.3390/rs11040420

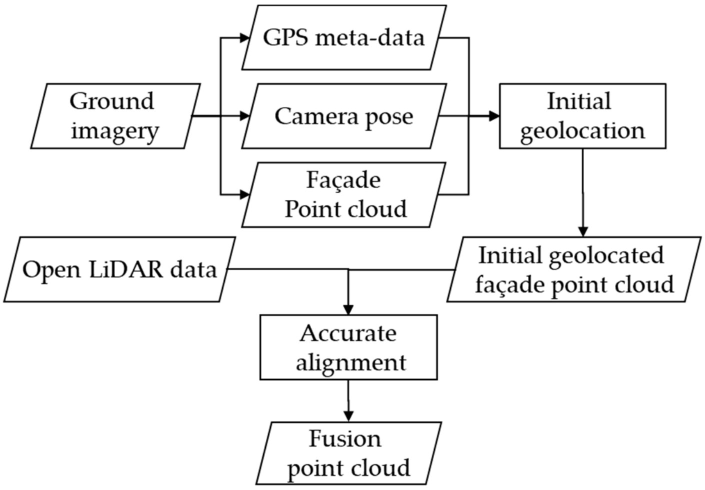

Figure 1. The overview of the proposed method.

The remainder of this paper is structured as follows. In section 2, we describe our approach for aligning façade point cloud generated from ground images to open LiDAR data. Section 3 presents the test results and discusses its performance. Finally, we conclude in section 4.

2. Methodology

Given ground image set $\{\boldsymbol{I}_i | i = 1,2,\ldots G\}$, COLMAP [32], a general-purpose Structure-from-Motion (SfM) and Multi-View Stereo (MVS) pipeline, is used to generate the facade point cloud $\boldsymbol{\mathcal{M}}^{loc}$ and camera positions $\{\boldsymbol{C}_i^{loc} | i = 1, 2, \ldots G\}$ in SfM local coordinate system. Additionally, the GPS meta-information $\{\boldsymbol{C}_i^{GPS} | i = 1, 2, \ldots G\}$ of these images are extracted from the EXIF information of $\{\boldsymbol{I}_i\}$. Corresponding to the capture area of $\{\boldsymbol{I}_i\}$, the open LiDAR data $\boldsymbol{\mathcal{P}}^{geo}$ with precise geographic coordinates are also given.

$\boldsymbol{\mathcal{P}}^{geo}$, $\boldsymbol{\mathcal{M}}^{loc}$, $\{\boldsymbol{C}_i^{GPS}\}$ and $\{\boldsymbol{C}_i^{loc}\}$ are taken as the input. The facade point cloud $\boldsymbol{\mathcal{M}}^{geo}$ accurately aligned to the corresponding open LiDAR data $\boldsymbol{\mathcal{P}}^{geo}$ is the ultimate output. The whole alignment process is performed in a two-step strategy: First, an initial georegistration is performed by approximately transforming $\boldsymbol{\mathcal{M}}^{loc}$ into the geo-referenced coordinate system according to a matching between $\{\boldsymbol{C}_i^{loc}\}$ and $\{\boldsymbol{C}_i^{GPS}\}$. Second, a modified Coherent Point Drift algorithm with normal consistency (NC-CPD) is proposed to accurately align the façade point cloud to open LiDAR data.

2.1. *Initial Georegistration*

Since the alignment between facade point cloud $\boldsymbol{\mathcal{M}}^{loc}$ in the local coordinate system and open LiDAR data $\boldsymbol{\mathcal{P}}^{geo}$ in geo-referenced coordinate system features large scale, translation and rotation differences, a georegistration is performed to approximately transform $\boldsymbol{\mathcal{M}}^{loc}$ to geo-referenced coordinate to reduce these differences at first.

Levelling the Facade Point Cloud. As a first step in the initial georegistration, we level the facade point cloud $\boldsymbol{\mathcal{M}}^{loc}$ to the upright direction (the opposite of the gravity vector) by estimating the upright vector $\boldsymbol{D}_{up}$ on the assumption that $\boldsymbol{D}_{up}$ should be perpendicular to the normal vectors of all façade points in $\boldsymbol{\mathcal{M}}^{loc}$. An initial upright vector $\overline{\boldsymbol{D}}_{up}$ is calculated by fitting a plane to the camera positions $\{\boldsymbol{C}_i^{loc}\}$ obtained in SfM process on the assumption that images are captured approximately on one plane. Then, candidate façade points $\{p_i\}$ whose normal vectors $\boldsymbol{N}_{p_i}$ are approximately perpendicular to $\overline{\boldsymbol{D}}_{up}$, in other words $|\boldsymbol{N}_{p_i}{}^T\overline{\boldsymbol{D}}_{up}| < 0.3$, are extracted. After that, a RANSAC-based approach is applied to refine the accurate upright vector $\boldsymbol{D}_{up}$ by iteratively selecting two points from candidate façade points and estimating the cross products of their normal vectors. Finally, leveling

Preprints (www.preprints.org) | NOT PEER-REVIEWED | Posted: 16 October 2018 doi:10.20944/preprints201810.0354.v1

Peer-reviewed version available at *Remote sensing* **2019**, *11*, 420; doi:10.3390/rs11040420

facade point cloud $\overline{\mathcal{M}}^{loc}$ is acquired by rotating $\mathcal{M}^{loc}$ to make the Z-axis in its coordinate system parallel to $\boldsymbol{D}_{up}$.

Geolocation of Leveling Facade Point Cloud using GPS meta-data. Since the SfM procedure has recovered the facade point cloud as well as cameras (images) shooting positions in the same local coordinate system, the problem of geolocating the facade point cloud can be converted into the problem of locating the SfM camera positions to the geo-referenced coordinate system, as shown in Figure 2. Due to GPS positioning features a dramatic accuracy difference between horizontal and altitude direction, a planar transformation and a vertical translation is calculated respectively.

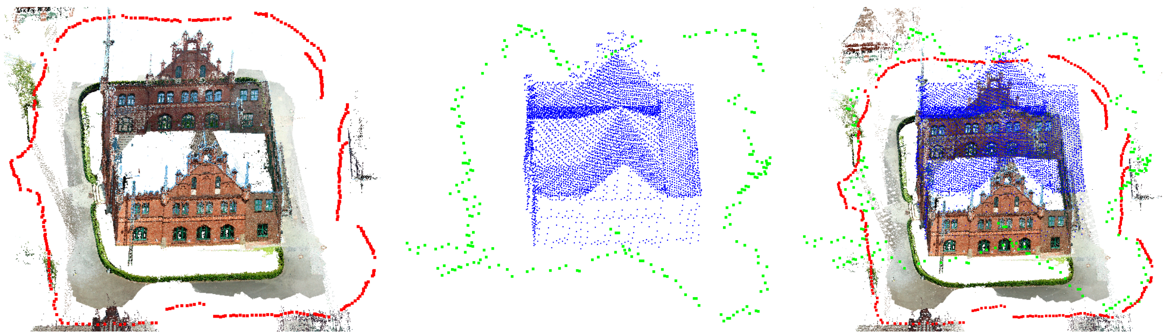

(a) (b) (c)

Figure 2. The overview of the initial georegistration process. Camera positions calculated in SfM (Red points in Figure. a) and camera GPS meta information (Green points in Figure. b) are matched using a RANSAC-based similarity transformation. Simultaneously, the facade point cloud (textured points in Figure. a) is aligned to point cloud of building from the open LiDAR data (blue points in Figure. b) by using the calculated similarity transformation parameters. The alignment result is shown in Figure. c.

A RANSAC-like 2D similarity transformation is estimated between the camera positions' x-y coordinates in local SfM coordinate and their corresponding longitude and latitude of GPS: Given the local coordinates $\{\boldsymbol{C}_i^{loc-2D}\}$ and the geo-referenced coordinates $\{\boldsymbol{C}_i^{GPS-2D}\}$ of the ground cameras, the minimal subset (size 3) of the ground cameras for point sets registration is selected from $\{\boldsymbol{C}_i^{loc-2D}\}$ and $\{\boldsymbol{C}_i^{GPS-2D}\}$ at random. Then, the 2D–2D similarity transformation is estimated using the least-squares solver, and the similarity transformation parameters are calculated. The inlier set of the estimated transformation is obtained with the inlier threshold ε. This process is repeated to obtain the maximal consensus set, which has the maximal number of inliers. Finally, the similarity transformation $\{s_{ca}^{2D}, \boldsymbol{R}_{ca}^{2D}, \boldsymbol{T}_{ca}^{2D}\}$ for geolocating the cameras (images) as well as the facade point cloud into the geo-referenced coordinate system is estimated with this maximal consensus set using the least-square method again. This procedure is formulated in Equation 2.

$$\begin{cases} \boldsymbol{C}_i^{GPS-2D} = s_{ca}^{2D}\, \boldsymbol{R}_{ca}^{2D} \boldsymbol{C}_i^{loc-2D} + \boldsymbol{T}_{ca}^{2D}, \qquad i = 1, \ldots N \\ \widetilde{\mathcal{T}}(s_{ca}^{2D}, \boldsymbol{R}_{ca}^{2D}, \boldsymbol{T}_{ca}^{2D}) \leftarrow RANSAC(s_{ca}^{2D}, \boldsymbol{R}_{ca}^{2D}, \boldsymbol{T}_{ca}^{2D}) \end{cases} \tag{1}$$

Then, a vertical translation $\boldsymbol{T}_{ca}^{v}$ is calculated by matching the mean value of z coordinate in $\{\boldsymbol{C}_i^{loc}\}$ and mean value of altitude in $\{\boldsymbol{C}_i^{GPS}\}$. Finally, apply transformation $\{s_{ca}^{2D}, \boldsymbol{R}_{ca}^{2D}, \boldsymbol{T}_{ca}^{2D}\}$ to (x, y) coordinate of $\overline{\mathcal{M}}^{loc}$ and transformation $\{s_{ca}^{2D}, \boldsymbol{T}_{ca}^{v}\}$ to z coordinate of $\overline{\mathcal{M}}^{loc}$, initial geolocated facade point clouds $\widetilde{\mathcal{M}}^{geo}$ can be obtained.

Peer-reviewed version available at Remote sensing 2019, 11, 420; doi:10.3390/rs11040420

Scale, translation and rotation differences are greatly relieved after initial alignment as described above, although there are meter-level [33] alignment errors between the initial geolocated facade point cloud $\widetilde{\mathcal{M}}^{geo}$ and the open LiDAR point cloud $\mathcal{P}^{geo}$ due to the GPS location uncertainties.

2.2. Extended Coherent Point Drift with Normal Consistency (NC-CPD)

To further reduce the initial alignment errors, accurate alignment is necessary for obtaining reliable and precise correspondences between $\widetilde{\mathcal{M}}^{geo}$ and $\mathcal{P}^{geo}$. Because of inevitable noise points in facade point cloud, including noise points generated in the SfM and MVS procedure and noise points of other ground object such as trees, lamp-posts and passers-by, an improved CPD algorithm with normal consistency is used to register the two point clouds with noise and structure ambiguities.

Coherent Drift Algorithm. This algorithm was first introduced in [31] for considering the alignment of two point sets as a probability density estimation. Given two D-dimensional point sets $\boldsymbol{X}_{N\times D} = (\boldsymbol{x}_1, \dots, \boldsymbol{x}_N)$ and $\boldsymbol{Y}_{M\times D} = (\boldsymbol{y}_1, \dots, \boldsymbol{y}_M)$, CPD method considers the alignment of the two point sets as a probability density estimation problem where one point set represents the GMM centroids ($\boldsymbol{Y}_{M\times D}$) and the other one represents the data points ($\boldsymbol{X}_{N\times D}$). The rigid transformation $\boldsymbol{\mathcal{T}}(\boldsymbol{R}, s, \boldsymbol{T})$ that aligns GMM centroids $\boldsymbol{Y}_{M\times \mathrm{D}}$ to data points $\boldsymbol{X}_{N\times \mathrm{D}}$ are obtained by maximizing the GMM posterior probability for the data point $\boldsymbol{X}_{N\times \mathrm{D}}$ at the optimum. The GMM probability density function of CPD can be written as Equation 2:

$$p(\boldsymbol{x}) = \sum_{m=1}^{M+1} P(m)p(\boldsymbol{x}|m) \tag{2}$$

where $p(\boldsymbol{x}|m) = \frac{1}{(2\pi\sigma^2)^{D/2}} exp^{-\frac{1}{2\sigma^2}\|x-y_m\|^2}$ and a uniform distribution $p(\boldsymbol{x}|M+1) = 1/N$ is used to account for outliers and the weight of it is donated as ω $(0 \le \omega \le 1)$. $P(m) = 1/M$ for all GMM components. Then, the mixture model takes the form:

$$p(\boldsymbol{x}) = \omega\frac{1}{N} + (1-\omega)\frac{1}{M}\sum_{m=1}^{M} p(\boldsymbol{x}|m) \tag{3}$$

GMM centroids locations are re-parametrised by rigid transformation parameters $(\boldsymbol{R}, s, \boldsymbol{t})$. We can estimate them by maximizing the negative likelihood function:

$$E(\boldsymbol{R}, s, \boldsymbol{t}, \sigma^2) = -log\prod_{n=1}^{N} p(\boldsymbol{x}_n) = -\sum_{n=1}^{N} log\sum_{m=1}^{M+1} P(m)p(\boldsymbol{x}_n|m) \tag{4}$$

The correspondence probability is defined between two points $\mathbf{y}_\mathrm{m}$ and $\mathbf{x}_\mathrm{n}$ as the posterior probability of the GMM centroids given the data points: $P(m|\boldsymbol{x}_n) = P(m)p(\boldsymbol{x}_n|m)/p(\boldsymbol{x}_n)$

The estimation of parameters $(\boldsymbol{R}, s, \boldsymbol{t}, \sigma^2)$ can use the Expectation Maximization (EM) algorithm. The first step (E step) : predicts the value of parameters based on previous values $(\boldsymbol{R}, s, \boldsymbol{T})^{old}$ and then Bayes' theory is used to calculate a posteriori probability distributions as the following equation:

$$p_{mn} = P^{old}(m|\boldsymbol{x}_n) = \frac{p(\boldsymbol{x}_n|m)}{\sum_{k=1}^{M} p(\boldsymbol{x}_k|m) + (2\pi\sigma^2)^{D/2}\frac{\omega}{1-\omega}\frac{M}{N}} \tag{5}$$

The second step (M step): obtain new parameters by minimising negative logarithm likelihood function of Equation 4. The EM algorithm proceeds by alternating between E and M-steps until convergence. After ignoring the constants independent of $(\boldsymbol{R}, s, \boldsymbol{t}, \sigma^2)$, it can be written as:

$$Q(\boldsymbol{R}, s, \boldsymbol{t}, \sigma^2) = \frac{1}{2\sigma^2}\sum_{n=1}^{N}\sum_{m=1}^{M} P^{old}(m|\boldsymbol{x}_n)\|\boldsymbol{x}_n - \mathcal{T}(y_m, \boldsymbol{R}, s, \boldsymbol{T})\|^2 + \frac{N_P D}{2}\log\sigma^2 \tag{6}$$

where $N_P = \sum_{n=1}^{N}\sum_{m=1}^{M} P^{old}(m|\boldsymbol{x}_n)$. For detailed solution process, please refer to [31].

Preprints (www.preprints.org) | NOT PEER-REVIEWED | Posted: 16 October 2018 doi:10.20944/preprints201810.0354.v1

Peer-reviewed version available at Remote sensing 2019, 11, 420; doi:10.3390/rs11040420

Coherent Point Drift with Normal Consistency. Though the original CPD algorithm achieves promising registration results in the situation of some noise and missing points, it may fail to handle the situation of ambiguities induced by repetitive and symmetric scene elements of buildings, as shown in Figure 3.(c). To resolve this problem, in other words, to avoid facade point cloud from registering to the ambiguities part, we introduce normal consistency into the original CPD algorithm to suppress aligning to ambiguities part by considering the normal direction of corresponding points.

The normalized normal $N_{\mathcal{P}_i}$ of 2D boundary points (detail introduced in section 2.2.3) extraction from open LiDAR data can be estimated according to their neighbor points (normal direction is toward the exterior of buildings), as shown in Figure 3. (a). The normalized normal $N_{\mathcal{M}_i}$ of 2D façade points (detail introduced in section 2.2.3) extraction from the facade point cloud is generated as a by-product in the MVS process so that it can be obtained without estimation, as shown in Figure 3. (b). We assume that the facade point cloud is correctly aligned to the actual part of the open LiDAR data only if $N_{\mathcal{M}_i} \cdot N_{\mathcal{P}_i} > 0$ is satisfied, in other words, the included angle between $N_{\mathcal{M}_i}$ and $N_{\mathcal{P}_i}$ should be less than 90 degrees, as shown in Figure 3. (d).

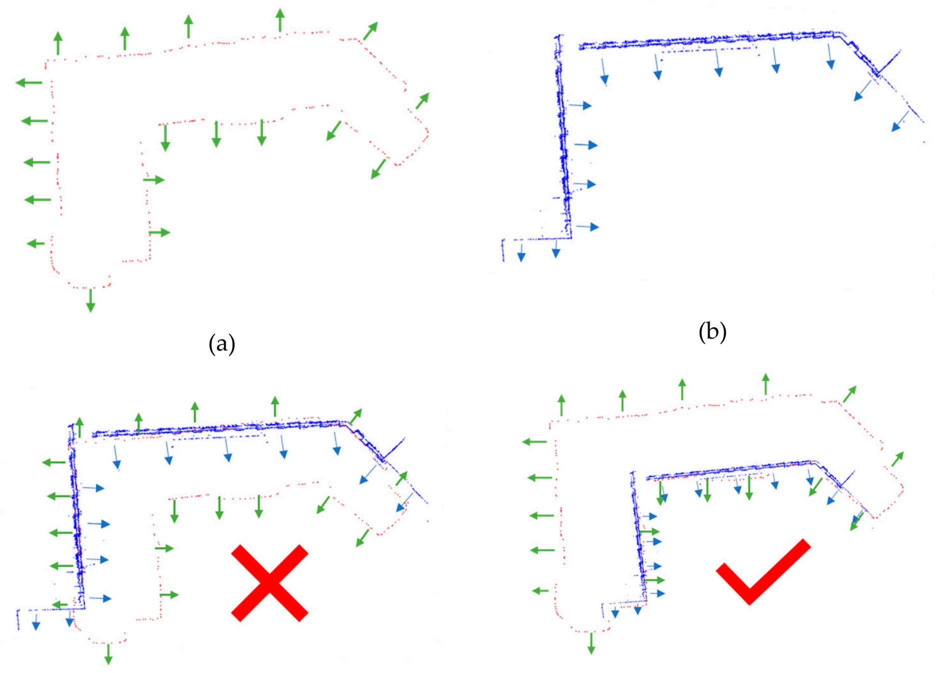

(a) (b) (c) (d)

Figure 3. Illustration of the wrong alignment caused by ambiguities. Fig (a) shows the 2D boundary points (red points) and their normal $N_{\mathcal{P}_i}$ (green lines with arrow). (b) shows the 2D façade points (blue points) and their normal $N_{\mathcal{M}_i}$ (blue lines with arrow). The alignment result in (c) is wrong for the big difference of normal direction in overlapping part of the two point clouds. The alignment results in (d) is correct for the high similarity in the normal direction of points in the overlapping part.

In the original CPD algorithm, a Gaussian distribution is used to model the likelihood of each centroid $p(\boldsymbol{x}|m)$. To avoid aligning facade point cloud to ambiguities part of open LiDAR data, corresponding priority based on normal consistency is introduced to decrease the likelihood when they are aligned to the ambiguities. To tolerate errors in estimating $N_{\mathcal{M}_i}$ *and* $N_{\mathcal{P}_i}$, we assign the dot product of $N_{\mathcal{M}_i}$ and $N_{\mathcal{P}_i}$ to 1 if the angle between $N_{\mathcal{M}_i}$ and $N_{\mathcal{P}_i}$ is less than 45 degree, or $N_{\mathcal{M}_i} \cdot N_{\mathcal{P}_i} \geq 0.7$ is satisfied, as shown in the following equation:

$$S = \begin{cases} exp^{-\frac{\left|N_{\mathcal{M}_i} \cdot N_{\mathcal{P}_i} - 1\right|^2}{2\varphi^2}} & N_{\mathcal{M}_i} \cdot N_{\mathcal{P}_i} < 0.7 \\ 1 & N_{\mathcal{M}_i} \cdot N_{\mathcal{P}_i} \geq 0.7 \end{cases} \tag{7}$$

where φ is the standard deviation of all $\left|N_{\mathcal{M}_i} \cdot N_{\mathcal{P}_i} - 1\right|$. Then, the likelihood of centroids is modified as following:

$$p(\boldsymbol{x}|m) = S \cdot \frac{1}{(2\pi\sigma^2)^{D/2}} \cdot exp^{-\frac{\|x_n - y_m\|^2}{2\sigma^2}} \tag{8}$$

When $S = 1$, the corresponding priority of each centroid is same, and NC-CPD degenerated to the original CPD algorithm.

2.3. Accurate alignment using NC-CPD

Although overlaps between $\widetilde{\mathcal{M}}^{geo}$ and $\mathcal{P}^{geo}$ in 3D space is hard to be found, 2D façade point overlaps can be accurately extracted at most of the time. We decompose the accurate alignment into a horizontal transformation and a vertical transformation, as shown in Figure 4.

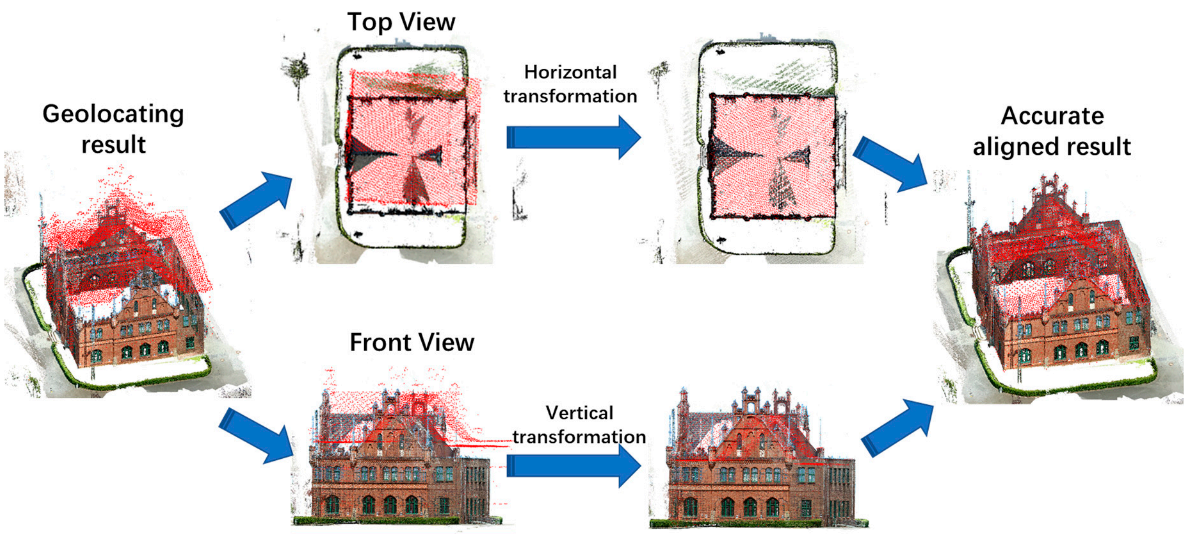

Figure 4. Overview of the accurate alignment process.

2D Façade Points Extraction from The Facade point cloud. Although most of the points in the facade point cloud generated from ground images are on the façade part, there are inevitably many noise points (such as trees, lamp-posts and passers-by), which will adversely affect the alignment. So, it is essential to extract the real facade points from the facade point cloud, to reduce the adverse effect of the noise points. Firstly, we extract candidate façade points of facade point cloud $\widetilde{\mathcal{M}}^{geo}$ by using the normal information. Since facade point cloud $\widetilde{\mathcal{M}}^{geo}$ has been set to the upright direction in section 2.1.1, the dot product of normal N_{p_i} of façade point p_i and the upright vector (Z axis) should be close to zero in an ideal case. Considering the error in the step of setting facade point cloud to upright, we modify the condition to $N_{p_i}{}^T \boldsymbol{Z}_{axis} < 0.01$. Then, we refine the candidate façade points by using their neighbour information. For each point $p_i(x_i, y_i, z_i)$ in $\widetilde{\mathcal{M}}^{geo}$, it is considered as a façade point only if its neighbour points $\{n_i(\hat{x}_i, \hat{y}_i, \hat{z}_i)\}$ satisfy the following conditions:

Preprints (www.preprints.org) | NOT PEER-REVIEWED | Posted: 16 October 2018 doi:10.20944/preprints201810.0354.v1

Peer-reviewed version available at Remote sensing 2019, 11, 420; doi:10.3390/rs11040420

$$\begin{cases} \sqrt{(x_{n_i}-x_{p_i})^2+(y_{n_i}-y_{p_i})^2}<0.1 \\ \dfrac{(\max\{z_i\}-\min\{z_i\})}{2}<\max\{\hat{z}_i\}-\min\{\hat{z}_i\} \\ \mathrm{count}\{n_i\}>10 \end{cases} \tag{9}$$

The above equation means that real façade points should contain enough number of neighbourhood points while these neighbourhood points' height should distribute within a certain range on the vertical direction. After the two steps, façade points $\widetilde{\boldsymbol{\mathcal{M}}}_f^{geo}$ are extracted from facade point cloud $\widetilde{\boldsymbol{\mathcal{M}}}^{geo}$ and most noise point such as ground, grass, trees, lamp-posts and passers-by are removed. Then, we project all points of $\widetilde{\boldsymbol{\mathcal{M}}}_f^{geo}$ into the plane of $Z=0$ to obtain 2D façade points $\widetilde{\boldsymbol{\mathcal{M}}}_{f2D}^{geo}$, as shown in Figure 5.(d).

2D Boundary Points Extraction of Open Lidar Data. Alpha shape algorithm [34] is used to find the boundary points from 2D LiDAR point cloud $\boldsymbol{\mathcal{P}}_{2D}^{geo}$ which is obtained by projecting LiDAR data into to the horizontal plane. Firstly, alpha shapes with all possible alpha radius $\{R_i|i\in(1,N)\}$ for $\boldsymbol{\mathcal{P}}_{2D}^{geo}$ are calculated. Then, once we find the critical alpha radius R_c which can create a single region for alpha shape, all alpha values above R_c can be extracted as candidate alpha values $\{R_k\}$. Secondly, we use a parameter W to select one alpha value R_f from $\{R_k\}$. Finally, the holes are filled after creating the final alpha shape with alpha value R_f. The points in the final alpha shape are considered as the boundary point set $\boldsymbol{\mathcal{P}}_{b2D}^{geo}$, as shown in Figure 5.(b).

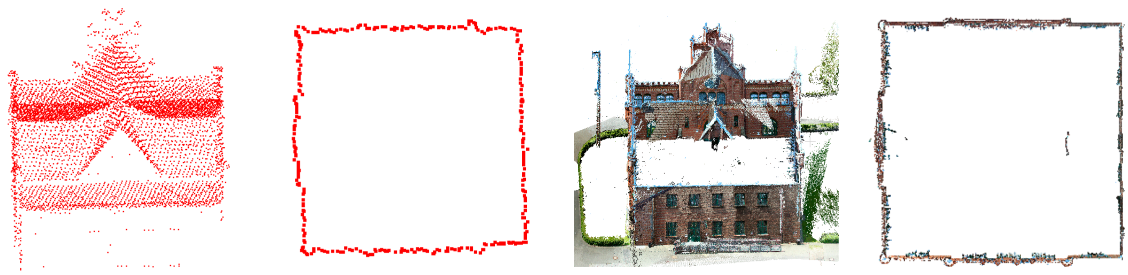

(a) (b) (c) (d)

Figure 5. Results of 2D façade points extraction and 2D boundary points extraction. Figure (a) and (c) show the open LiDAR data and facade point cloud respectively. Figure (b) shows the boundary points (top view) extracted from open LiDAR data and (d) shows the façade points (top view) extracted from the facade point cloud.

Horizontal Alignment Using NC-CPD. From previous steps, 2D boundary points $\boldsymbol{\mathcal{P}}_{b2D}^{geo}$ and 2D façade points $\widetilde{\boldsymbol{\mathcal{M}}}_{f2D}^{geo}$ are extracted from open LiDAR data and facade point cloud, respectively. NC-CPD algorithm described in detail in section 2.2.2 is used to matching $\widetilde{\boldsymbol{\mathcal{M}}}_{f2D}^{geo}$ to $\boldsymbol{\mathcal{P}}_{b2D}^{geo}$. Firstly, we calculate initial σ^2 with $\boldsymbol{R}=\boldsymbol{I}, s=1,\ \boldsymbol{t}\ =\boldsymbol{0}.$ Initial S in Equation (7) is also calculated with $\boldsymbol{N}_{\mathcal{P}_i}$ and initial $\boldsymbol{N}_{\mathcal{M}_i}$. Then, $P^{old}(m|\boldsymbol{x}_n)$ in Equation (5) is calculated using $\boldsymbol{R}, s, \boldsymbol{t}, \sigma^2, S$. Substitute $P^{old}(m|\boldsymbol{x}_n)$ into Equation (6), $\boldsymbol{R}$, s, $\boldsymbol{T}$, σ^2 can be updated by minimizing Q in Equation (6). New S can also be calculated by using new $\boldsymbol{N}_{\mathcal{P}_i}^{new}=\boldsymbol{N}_{\mathcal{P}_i}\cdot\boldsymbol{R}^T$. Repeat the previous steps until Q does not change too much or a certain number of iterations is reached. After applying final transformation parameters $(\boldsymbol{R}, s, \boldsymbol{t})$ to x and y coordinates of $\widetilde{\boldsymbol{\mathcal{M}}}^{geo}$, accurately aligned facade point cloud $\boldsymbol{\mathcal{M}}_{f2D}^{geo}$ on

Preprints (www.preprints.org) | NOT PEER-REVIEWED | Posted: 16 October 2018 doi:10.20944/preprints201810.0354.v1

Peer-reviewed version available at Remote sensing 2019, 11, 420; doi:10.3390/rs11040420

X and Y axis direction are obtained. The registration process of NC-CPD is described in detail in Figure 6.

Algorithm: Horizontal Alignment Using NC-CPD

Input: 2D boundary points $\boldsymbol{\mathcal{P}}_{b2D}^{geo}$ and corresponding normal vector $\boldsymbol{N}_{\mathcal{P}_i}$

2D façade points $\widetilde{\boldsymbol{\mathcal{M}}}_{f2D}^{geo}$ and corresponding initial normal vector $\boldsymbol{N}_{\mathcal{M}_i}$

Output: Accurate geolocated 2D façade points $\boldsymbol{\mathcal{M}}_{f2D}^{geo}$

- **Initialization**: Assign coarse alignment results: $\boldsymbol{R} = \boldsymbol{I}, s = 1,\ \boldsymbol{t} = \boldsymbol{0}$,
  Calculate initial σ^2: $\sigma^2 = \frac{1}{2NM}\sum_{n=1}^{N}\sum_{m=1}^{M}||\boldsymbol{\mathcal{P}}_n - \boldsymbol{\mathcal{M}}_m||^2$,
  Construct initial normal consistency S in Equation. (7)
- **EM optimization**. repeat until convergence to obtain the final $\boldsymbol{R_f},\ s_f,\ \boldsymbol{t_f},\ \sigma^2$
  - ⇨ E-step: Update $p(m|\boldsymbol{x}_n)$ with $\boldsymbol{R}, s, \boldsymbol{T}, \sigma^2, S$
  - ⇨ M-step: solve for the new $\boldsymbol{R}, s, \boldsymbol{T}, \sigma^2$ by minimizing Equation. (6)
- The aligned 2D façade points is $\boldsymbol{\mathcal{M}}_{f2D}^{geo} = s_f \widetilde{\boldsymbol{\mathcal{M}}}_{f2D}^{geo} \boldsymbol{R}_f^{T} + \boldsymbol{t}_f^{T}$

Figure 6. The algorithm of horizontal alignment using CPD with normal consistency.

Then, after updating Z coordinates of façade points by applying s *and* t, 3D façade point cloud $\ddot{\boldsymbol{\mathcal{M}}}^{geo}$ is obtained.

Vertical Alignment. Façade point cloud has been accurately aligned to open LiDAR data on X and Y axis direction by the horizontal alignment described in the previous section. A translation T_z on the vertical direction between $\ddot{\boldsymbol{\mathcal{M}}}^{geo}$ and $\boldsymbol{\mathcal{P}}^{geo}$ remain to be calculated. We calculate optimal T_z by matching corresponding boundary points respectively from $\boldsymbol{\mathcal{P}}^{geo}$ and $\ddot{\boldsymbol{\mathcal{M}}}^{geo}$ on the Z axis direction, as following steps: (1). For one point $\bar{p}_i(x_i, y_i)$ in 2D boundary points $\boldsymbol{\mathcal{P}}_{b2D}^{geo}$, we find 2D neighbour point set $\{p_1, \ldots, p_i\}$ and $\{q_1, \ldots, q_j\}$ of $\bar{p}_i$ with radius 0.1 meter, respectively from $\boldsymbol{\mathcal{P}}^{geo}$ and $\ddot{\boldsymbol{\mathcal{M}}}^{geo}$. (2). Find the point p_m and q_n with maximum value on Z axis, respectively from $\{p_1, \ldots, p_i\}$ and $\{q_1, \ldots, q_j\}$, then calculate height difference $T_i = z_{p_m} - z_{q_n}$. (3). For other point in $\boldsymbol{\mathcal{P}}_{b2D}^{geo}$, repeat step (1) (2) to obtain height difference set $\{T_1, \ldots, T_i\}$. Then, the optimal T_z is calculated by fitting height difference set $\{T_1, \ldots, T_i\}$. Finally, applying translation T_z to z coordinate of $\ddot{\boldsymbol{\mathcal{M}}}^{geo}$, accurately aligned facade point cloud $\boldsymbol{\mathcal{M}}^{geo}$ is obtained in the end.

3. Experiments and Discussion

3.1. Datasets Description

So far, there are currently no available benchmark datasets for fusing airborne LiDAR data and facade point cloud generated from images. The proposed method is evaluated on a combined dataset:

1. Open LiDAR data of Dortmund in German which contain three experimental buildings (Rathaus, Lohnhalle, Verwaltung) are downloaded from a Germany open data download portal [7]. These open LiDAR data have been geolocated in the ETRS89 reference system with a UTM projection with a point density of 25 points/m².

2. Ground images of the three buildings come from a part of a benchmark dataset named "ISPRS benchmark on multi-platform photogrammetry" [35] which can be downloaded from the official website of ISPRS. These images are captured around the buildings using high-resolution digital cameras on the ground. Due to the use of GPS locating accessories, image shooting positions are recorded in these JPEG format images as GPS meta-data. Global coordinates of targets centers distributed on the façade of the three buildings are provided for accuracy estimation. The details of these image collections are listed in Table 1.

Table 1. Details of ground image datasets

	Rathaus	Lohnhalle	Verwaltung
Images number	1211	194	351
Façade model points	36,085,050	8,004,604	11,176,836
Capturing device	SONY NEX-7	Canon EOS 600D	Canon EOS 600D
Focal length	16 mm	20mm	20mm
Image size (pixel)	4000 × 6000	5184 × 3456	5184 × 3456
Ground resolution	7.6 mm/pixel	3.1 mm/pixel	1.72 mm/pixel
GPS information	✓	✓	✓
With GCP	✓	✓	✓

3.2. Qualitative Analysis

As shown in Figure 7, facade point clouds of Rathaus, Lohnhalle, Verwaltung (Figure.7 B1, B2, B3) are generated from ground images (Figure.7 A1, A2, A3, image sample) using SfM and MVS algorithms in COLMAP [32]. The open LiDAR data of the three buildings are visualized by height rendering map in Figure.7 C1, C2, C3. It can be seen that there are no overlaps between open LiDAR data and facade point clouds on their façade part except for Verwaltung, which has a small number of points on the façades. But from another perspective, open LiDAR data and facade point clouds are complementary, the former lack structural details on the façades, while the latter lack roof information.

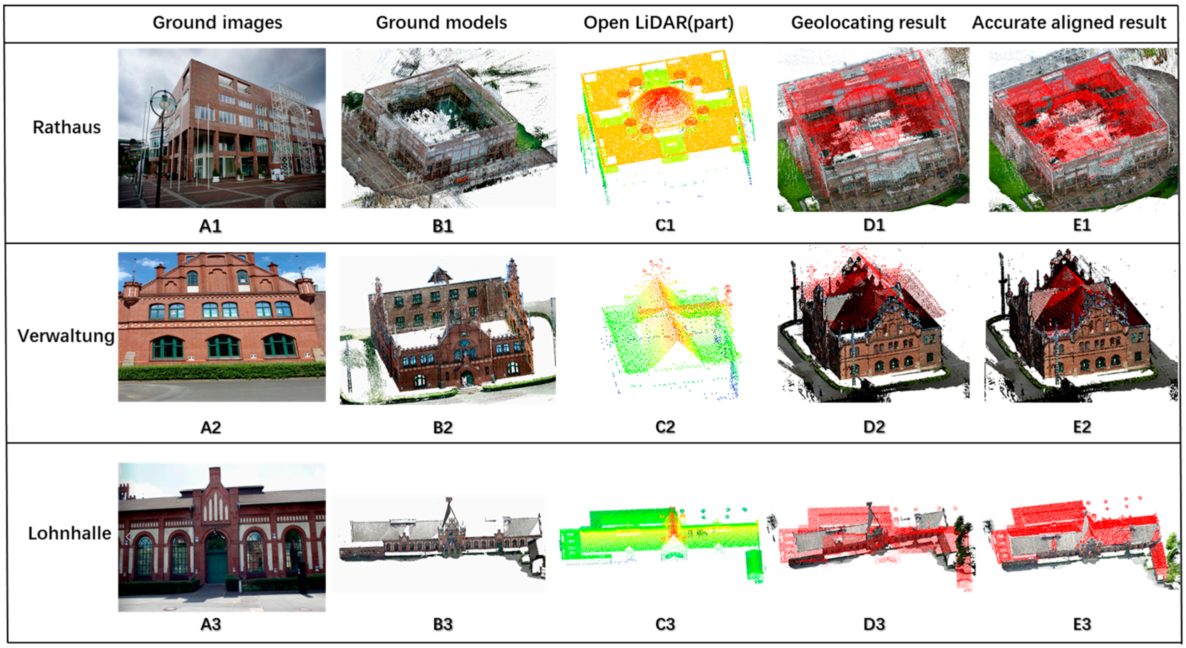

Figure 7. Datasets for evaluating the proposed method. From top to bottom, the different rows respectively show the ground images (A), facade point clouds (B), open LiDAR (C), coarse alignment result (D) and accurate alignment result (E) of Rathaus, Verwaltung and Lohnhalle.

The initial geolocation results which are not entirely accurate due to the low accuracy of GPS are shown in Figure.7 D1, D2, D3, D4 (the red colour is assigned to open LiDAR data for better recognition). After performing the accurate alignment step, the facade point clouds and open LiDAR data are aligned well, as shown in Figure.7 E1, E2, E3. We also test the matching of our datasets using

Preprints (www.preprints.org) | NOT PEER-REVIEWED | Posted: 16 October 2018 doi:10.20944/preprints201810.0354.v1

Peer-reviewed version available at *Remote sensing* **2019**, *11*, 420; doi:10.3390/rs11040420

ICP and NDT algorithm, two classical algorithms of point set registration. The visualising results are shown in Figure 8. Because of a relatively good density of points on the façades, we can see that ICP and NDT achieve a relatively well result in Verwaltung comparing with Rathaus, Lohnhalle.

Surface reconstruction (Figure.9) was performed using the method in [36] to demonstrate the effectiveness of our alignment algorithm. Both completeness and structural details are achieved in the surface reconstruction after accurately aligning the facade point cloud to open LiDAR data.

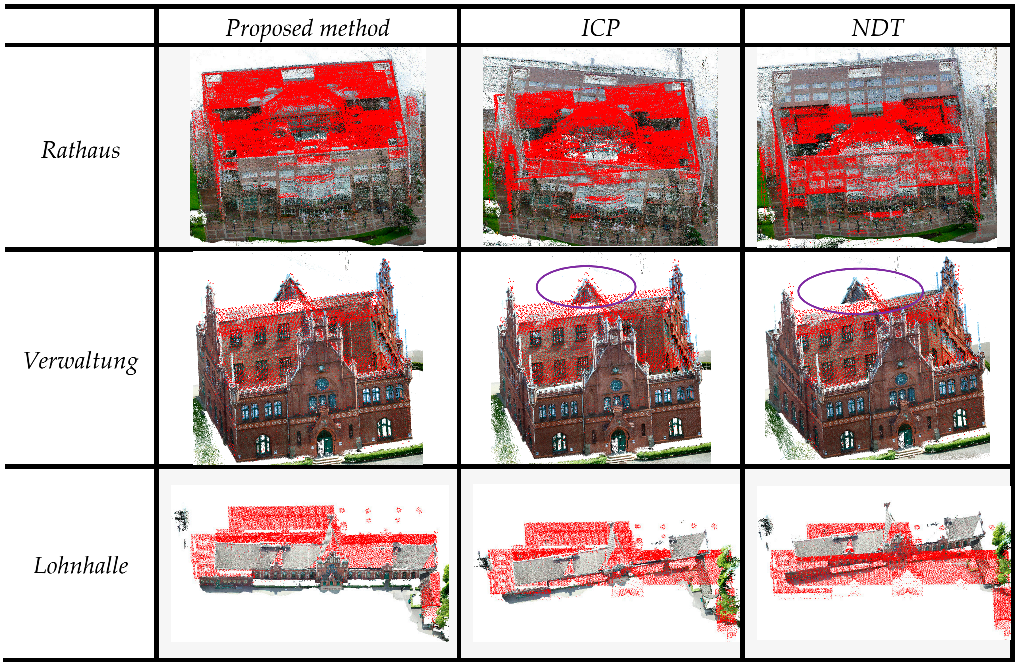

Figure 8. Fusion results of the proposed method comparing with ICP and NDT methods.

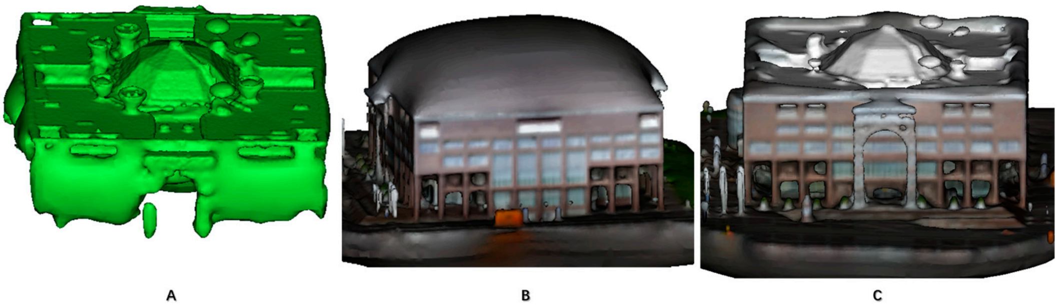

Figure 9. Poisson Surface reconstruction results. (a) Poisson Surface reconstruction from open LiDAR data. (b). Poisson Surface reconstruction from façade point cloud generated from ground images. (c). Poisson Surface reconstruction from fusion point cloud of open LiDAR data and façade point cloud.

3.2. Quantitative Analysis

As shown in section 2.2, an iteration process is performed in the EM process to find the optimal alignment result. After about less than 30 times iteration, the ratio of Q to initial Q_0 quickly decline to 1%, as shown in Figure 10. (a). Provided in the dataset of 'ISPRS benchmark on multi-platform photogrammetry', accurate geographical coordinates $\{GCP_i\}$ of target centers distributed on the façade are used for quantitative evaluations of the alignment results, as shown in Figure 10.(b). We estimate RMSE (root mean square error), mean errors and standard deviation between provided global coordinates of target centers and their coordinates in the aligned results from different methods, as shown in Table 2.

Preprints (www.preprints.org) | NOT PEER-REVIEWED | Posted: 16 October 2018 doi:10.20944/preprints201810.0354.v1

Peer-reviewed version available at Remote sensing 2019, 11, 420; doi:10.3390/rs11040420

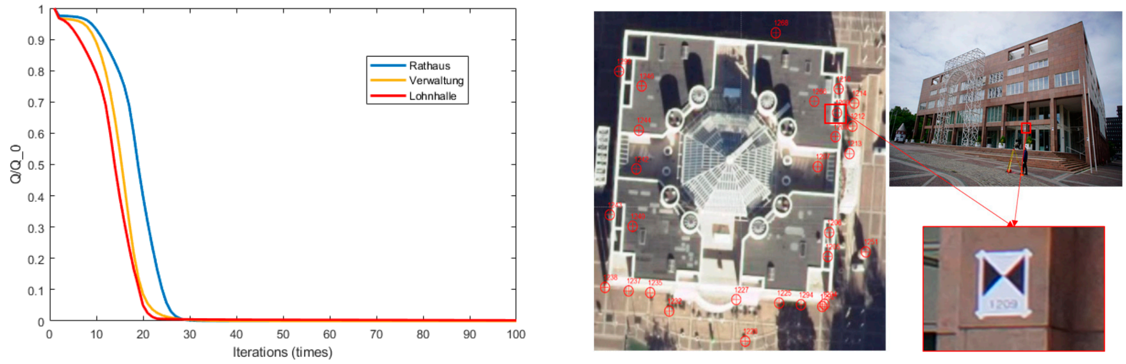

(a) (b)

Figure 10. (a) Change of Q after each iteration. (b) Illustration of ground targets.

In fact, the error in the final geolocated facade point cloud includes errors from both the facade point cloud generating process and the registration process. It is difficult to estimate the accuracy of the registration process alone. In order to find the optimal geolocated results of façade point cloud which include almost no registration errors, target centres registration (TCR) is performed by estimating the rigid transformation $\mathcal{T}(\boldsymbol{R}, s, \boldsymbol{T})$ between the local coordinates of manually picked out target centres and their provided global coordinates $\{GCP_i\}$ using the least-square method. Due to greatly reducing the registration errors by direct use of high-precision GCPs, errors in geolocating the façade point cloud using TCR method can be referenced as errors from the facade point cloud generating process.

Table 2. RMSE, ME and SD of the proposed method compared with other methods.

	Targets Qty	Methods	RMSE (m)	Mean Error (m)	Standard Deviation (m)
Rathaus	25	TCR	0.192	0.164	0.197
		Proposed method	**0.389**	**0.342**	**0.304**
		ICP	4.283	3.548	4.280
		NDT	1.876	1.231	1.631
Verwaltung	40	TCR	0.049	0.030	0.050
		Proposed method	**0.185**	**0.161**	**0.173**
		ICP	0.336	0.288	0.300
		NDT	1.700	1.452	1.489
Lohnhalle	32	TCR	0.188	0.164	0.189
		Proposed method	**0.468**	**0.380**	**0.423**
		ICP	10.039	8.537	5.672
		NDT	23.225	22.336	6.495

By analysing the errors of the different methods in Table 2, we can see that the proposed method significantly improves the accuracy of test datasets comparing with ICP and NDT. It is well known that Iterative Closest Point (ICP) [25] and Normal-Distributions Transform (NDT) [37] are effective methods of point sets registration with large overlaps. Experiments have shown that ICP and NDT methods cannot handle our datasets in which almost no overlaps can be found. So, errors up to 10 meters are obtained except for dataset of Verwaltung, which have a small number of points on the façade parts. Although not as good as the result of TCR methods, the proposed method achieves the best accuracy compared to ICP and NDT methods due to the use of similarity on 2D outlines of buildings. The accuracy of the proposed method is highly correlated with quality of façade point cloud generated from images. For Rathaus, the farthest mean capture distance leads to an apparent worst quality of façade point cloud from captured images (most significant errors in TCR method). Consequently, a relatively large error appeared in dataset Rathaus using the proposed method. For Lohnhalle dataset, we believe the disclosure of images captured around the target building cause the relatively apparent errors in SfM process, even though the mean capture distance is much closer than that of Rathaus dataset. However, the quality of the façade point cloud generated from images is uncontrollable during the registration process, and how to improve it is beyond the scope of this article.

3.3. *Robustness Analysis*

It is known that different point densities and degrees of noise in the point clouds have a significant impact on the performance of registration. We take several experiments on point clouds mixed with different degrees of noise as well as point densities to test the robustness of the proposed method. Fig. 12a–b illustrates the registration results achieved by the proposed method under different degrees of noise and point densities.

Robustness to Point Densities. To evaluate the robustness of the proposed method to point density, we randomly down-sample facade point cloud of Rathaus, Verwaltung and Lohnhalle from their original point density to various densities. Different RMSEs evaluated between target centre coordinates at different point density are given in Figure. 12 a. It can be seen that the proposed method performed well even at 1% of the original point density, indicating the robustness of the proposed method to different point densities. We attribute the robustness of our approach to different point densities to the use of 2D similarity of building outlines in the registration between two sources of point clouds.

Robustness to Noise. To evaluate the robustness of the proposed method to noise, Gaussian noise with different standard deviations (1, 2, 3, 4, and 5 cm) was added to the point cloud data. The different RMSE evaluated between target center coordinates under different levels of noise are shown in Figure. 12b. Even when Gaussian noise with a standard deviation of 5 cm is added to the point cloud, the proposed method achieved fine and stable accuracy. It indicates that the proposed method is very robust to different levels of noise. We attribute the robustness of our approach to different degrees of noise to the use of the probabilistic method in the accurate alignment.

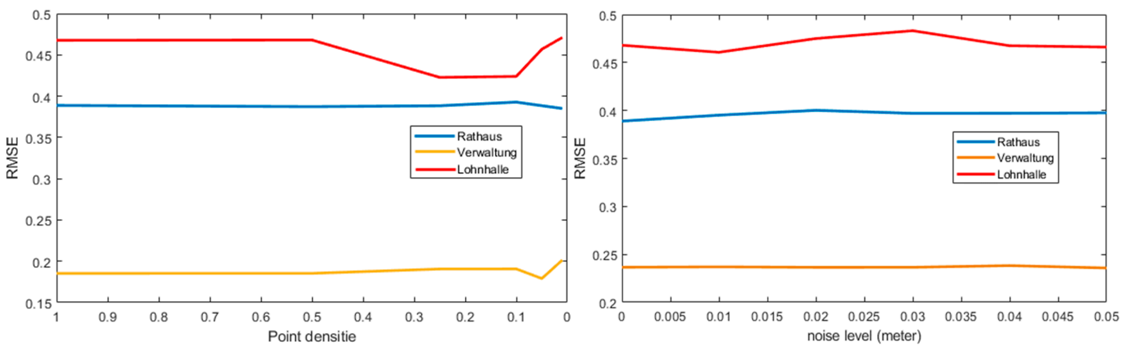

(a) (b)

Figure 11. Robustness analysis of the proposed method.

4. Conclusion and Future Work

This paper presents an accurate and efficient framework for improving building façade details of open LiDAR data using terrestrial images without ground control point. The critical step of this

Peer-reviewed version available at Remote sensing 2019, 11, 420; doi:10.3390/rs11040420

framework is the alignment between limited overlapped facade point cloud generated from ground images and open LiDAR point cloud. Experiments have shown that classic registration methods such as ICP and NDT cannot handle our datasets in which limited overlaps can be found. Comparing with ICP and NDT, the proposed method reduces the registration errors from up to 10 meters to less than half a meter. We believe that our approach achieves good accuracy for the following reasons:(1). Using Two-step strategies. Scale, translation and rotation differences are greatly relieved after coarse alignment using GPS information of images. (2). Decompose registration into a horizontal transformation and a vertical transformation instead of 3D registration directly. 2D overlapping points on the contour of buildings are more stable for registration of the façade point cloud and airborne point cloud than 3D overlapping points which can hardly be found between the two different sources of point clouds. (3). The NC-CPD inherits the noise robust property of original CPD algorithm. At the same time, it can handle the registration with structural ambiguities of buildings by introducing normal consistency into the original CPD algorithm.

Both completeness and structural details of buildings in the open LiDAR data are significantly improved after accurate alignment so that a complete and full resolution city building modelling and other applications can be achieved. Our method can be extended to acquire images of different buildings via crowdsourcing for improving façades details for open LiDAR data at city-scale. In the future, we intend to carry larger trials with more terrestrial images of buildings via crowdsourcing. Despite working well on many datasets, our method relies heavily on high-quality façade point cloud generated from the SfM and MVS process in order to use the 2D outline information, which is the only similarity between the two building point clouds. As such, the completeness and correctness of façade point cloud require continuous improvement in image matching.

Acknowledgements: This work was partially supported by the National Natural Science Foundation of China (No. 41271431, No. 41801390).

Author Contributions: The work presented here was carried out in collaboration among all authors. All authors have contributed to this manuscript. Shenman Zhang is the primary author, having conducted the survey and written the content. Pengjie Tao contributes to the analyse and discussion of an experiment as well as writing and editing of the manuscript.

Conflicts of Interest: The authors declare no conflict of interest.

References

1. NYC Open Data. Available online: https://opendata.cityofnewyork.us/.
2. Open Data DC. Available online: http://opendata.dc.gov/.
3. Open Data of Canada. Available online: https://open.canada.ca/en/open-data.
4. Directive, I. N. S. P. I. R. E. Directive 2007/2/EC of the European Parliament and of the Council of 14 March 2007 establishing an Infrastructure for Spatial Information in the European Community (INSPIRE). *Publ. Off. J. 25th April* 2007.
5. European Data Portal. Available online: https://data.europa.eu.
6. Scottish Remote Sensing Portal. Available online: https://remotesensingdata.gov.scot/.
7. Open NRW. Available online: https://open.nrw/open-data/.
8. Langheinrich, M. Evaluation of Gmsh Meshing Algorithms in Preparation of High-Resolution Wind Speed Simulations in Urban Areas. *Int. Arch. Photogramm. Remote Sens. Spat. Inf. Sci.* 2018, *42*.
9. Kersting, N. Open Data, Open Government und Online Partizipation in der Smart City. Vom Informationsobjekt über den deliberativen Turn zur Algorithmokratie? In *Staat, Internet und digitale Gouvernementalität*; Springer, 2018; pp. 87–104.

10. Degbelo, A.; Trilles, S.; Kray, C.; Bhattacharya, D.; Schiestel, N.; Wissing, J.; Granell, C. Designing semantic application programming interfaces for open government data. *JeDEM - eJournal eDemocracy Open Gov.* 2016, *8*, 21–58.
11. Luebke, D.; Reddy, M.; Cohen, J. D.; Varshney, A.; Watson, B.; Huebner, R. Level of Detail for 3D Graphics : Application and Theory. 2002, 431.
12. Furukawa, Y.; Ponce, J. [PVMS] Accurate, Dense , and Robust Multiview Stereopsis. 2010, *32*, 1362–1376.
13. Agarwal, S.; Snavely, N.; Simon, I.; Seitz, S. M.; Szeliski, R. Building Rome in a day. *Proc. IEEE Int. Conf. Comput. Vis.* 2009, 72–79, doi:10.1109/ICCV.2009.5459148.
14. Shan, Q.; Curless, B.; Furukawa, Y.; Hernandez, C.; Seitz, S. M. Occluding contours for multi-view stereo. In *Proceedings of the IEEE Computer Society Conference on Computer Vision and Pattern Recognition*; 2014; pp. 4002–4009.
15. Goesele, M.; Snavely, N.; Curless, B.; Hoppe, H.; Seitz, S. M. Multi-view stereo for community photo collections xxx. *Proc. ICCV* 2007, 1–8, doi:10.1109/ICCV.2007.4408933.
16. Snavely, N.; Simon, I.; Goesele, M.; Szeliski, R.; Seitz, S. M. Scene reconstruction and visualization from community photo collections. *Proc. IEEE* 2010, *98*, 1370–1390, doi:10.1109/JPROC.2010.2049330.
17. Boulaassal, H.; Landes, T.; Grussenmeyer, P. Reconstruction of 3D Vector Models of Buildings By Combination of Als, Tls and Vls Data. *ISPRS - Int. Arch. Photogramm. Remote Sens. Spat. Inf. Sci.* 2012, *XXXVIII-5/*, 239–244, doi:10.5194/isprsarchives-XXXVIII-5-W16-239-2011.
18. Shan, Q.; Wu, C.; Curless, B.; Furukawa, Y.; Hernandez, C.; Seitz, S. M. Accurate geo-registration by ground-to-aerial image matching. *Proc. - 2014 Int. Conf. 3D Vision, 3DV 2014* 2015, 525–532, doi:10.1109/3DV.2014.69.
19. Wang, C.-P.; Wilson, K.; Snavely, N. Accurate georegistration of point clouds using geographic data. *3DTV-Conference, 2013 Int. Conf.* 2013, 33–40, doi:10.1109/3DV.2013.13.
20. Agarwal, S.; Furukawa, Y.; Snavely, N. Building rome in a day. *Commun. …* 2011, 105–112, doi:10.1145/2001269.
21. Rueckert, D.; Sonoda, L. I.; Hayes, C.; Hill, D. L.; Leach, M. O.; Hawkes, D. J. Nonrigid registration using free-form deformations: application to breast MR images. *712 Ieee Trans. Med. Imaging* 1999, *18*, 712–21.
22. El-Hakim, S. F.; Beraldin, J. A.; Picard, M.; Godin, G. Detailed 3D reconstruction of large-scale heritage sites with integrated techniques. *IEEE Comput. Graph. Appl.* 2004, *24*, 21–29, doi:10.1109/MCG.2004.1318815.
23. Yan, G.; Wen, D.; Olariu, S.; Weigle, M. C. Security challenges in vehicular cloud computing. In *IEEE Transactions on Intelligent Transportation Systems*; 2013; Vol. 14, pp. 284–294.
24. Goshtasby, A. A. *2-D and 3-D image registration: for medical, remote sensing, and industrial applications*; John Wiley & Sons, 2005; ISBN 0471724262.
25. Besl, P. J.; McKay, N. D. A Method for Registration of 3-D Shapes. *IEEE Trans. Pattern Anal. Mach. Intell.* 1992, *14*, 239–256.
26. Brun, A.; Westin, C. *Robust Generalized Total Least Squares*; Springer Berlin Heidelberg, 2004; ISBN 978-3-540-22976-6.
27. Chetverikov, D.; Stepanov, D.; Krsek, P. Robust Euclidean alignment of 3D point sets: the trimmed iterative closest point algorithm. *Image Vis. Comput.* **2005**, *23*, 299–309.

Preprints (www.preprints.org) | NOT PEER-REVIEWED | Posted: 16 October 2018 doi:10.20944/preprints201810.0354.v1

Peer-reviewed version available at *Remote sensing* **2019**, *11*, 420; doi:10.3390/rs11040420

28. Stewart, C. V.; Chia-Ling Tsai; Roysam, B. The dual-bootstrap iterative closest point algorithm with application to retinal image registration. *IEEE Trans. Med. Imaging* **2003**, *22*, 1379–1394, doi:10.1109/TMI.2003.819276.
29. Kaneko, S.; Kondo, T.; Miyamoto, A. Robust matching of 3D contours using iterative closest point algorithm improved by M-estimation. *Pr* **2003**, *36*, 2041–2047.
30. Campbell, D.; Petersson, L. An adaptive data representation for robust point-set registration and merging. *Proc. IEEE Int. Conf. Comput. Vis.* **2015**, *2015 Inter*, 4292–4300, doi:10.1109/ICCV.2015.488.
31. Myronenko, A.; Song, X. Point set registration: Coherent point drifts. *IEEE Trans. Pattern Anal. Mach. Intell.* **2010**, *32*, 2262–2275, doi:10.1109/TPAMI.2010.46.
32. Schonberger, J. L.; Frahm, J.-M. Structure-from-Motion Revisited. *2016 IEEE Conf. Comput. Vis. Pattern Recognit.* **2016**, 4104–4113, doi:10.1109/CVPR.2016.445.
33. GPS Accuracy Available online: https://www.gps.gov/systems/gps/performance/accuracy/.
34. Edelsbrunner, H.; Mücke, E. P. Three-dimensional alpha shapes. *ACM Trans. Graph.* **1994**, *13*, 43–72, doi:10.1145/174462.156635.
35. Nex, F.; Remondino, F.; Gerke, M.; Przybilla, H.-J.; Bäumker, M.; Zurhorst, A. ISPRS BENCHMARK FOR MULTI-PLATFORM PHOTOGRAMMETRY. *ISPRS Ann. Photogramm. Remote Sens. Spat. Inf. Sci.* **2015**, *2*.
36. Kazhdan, M.; Hoppe, H. Screened poisson surface reconstruction. *ACM Trans. Graph.* **2013**, *32*, 1–13, doi:10.1145/2487228.2487237.
37. Magnusson, M. The Three-Dimensional Normal-Distributions Transform --- an Efficient Representation for Registration, Surface Analysis, and Loop Detection. *Renew. Energy* **2009**, *28*, 655–663.